Earth and Planetary Science Letters 557 (2021) 116723

Contents lists available at ScienceDirect

Earth and Planetary Science Letters

www.elsevier.com/locate/epsl

Dynamic triggering of earthquakes in the North Island of New Zealand following the 2016 M_w 7.8 Kaikōura earthquake

Dongdong Yao [a,b,*], Zhigang Peng [b], Yoshihiro Kaneko [c,d], Bill Fry [c], Xiaofeng Meng [e]

[a] Earth and Environmental Sciences, College of Literature, Science, and the Arts, University of Michigan, Ann Arbor, MI, USA
[b] School of Earth and Atmospheric Sciences, Georgia Institute of Technology, Atlanta, GA, USA
[c] GNS Science, Lower Hutt, New Zealand
[d] Kyoto University, Kyoto, Japan
[e] Southern California Earthquake Center, University of Southern California, Los Angeles, CA, USA

ARTICLE INFO

Article history:
Received 10 April 2020
Received in revised form 4 December 2020
Accepted 14 December 2020
Available online xxxx
Editor: J.-P. Avouac

Keywords:
dynamic triggering
Kaikōura earthquake
Taupo Volcano Zone
slow-slip event
earthquake detection
dynamic stress modeling

ABSTRACT

Large earthquakes are capable of triggering microseismicity, deep tremor and slow-slip events from intermediate- to long-distance ranges. Unfortunately, earthquake catalogs are typically incomplete right after large mainshocks. Hence, mapping triggering patterns and understanding the underlying triggering mechanism are challenging. Here we present two different types of seismicity responses to dynamic stressing by passing seismic waves in the North Island of New Zealand following the 2016 M_w 7.8 Kaikōura earthquake. Based on a template matching technique, we identify up to 4-7 times more earthquakes than listed in New Zealand's GeoNet catalog. We also compute the dynamic stress perturbations in the North Island due to the Kaikōura mainshock and compare them to seismicity rate changes to identify regions with high susceptibility to dynamic stress triggering. Abundant triggered earthquakes occurred immediately following the mainshock in the shallow crust around the active Taupo Volcano Zone, likely related to activation of crustal faults/fluids associated with back-arc rifting and volcanism. Approximately 8 days after the initial dynamic stressing, an active burst of seismicity with the largest event of M_L 5.55 occurred along the shallow megathrust near Porangahau on the east coast of the North Island. This burst of seismicity is likely driven by a ~M_w 7.1 shallow slow slip event dynamically triggered by the mainshock. Our findings reveal the heterogeneous nature of dynamic triggering in a plate boundary region with recent large earthquake sequences and aseismic transient events and further highlight the difficulties in time-dependent earthquake forecasting following large mainshocks.

1. Introduction

Tectonic earthquakes occur when faults are critically stressed to failure. A major challenge in seismology is to accurately forecast the location and timing of potential damaging earthquakes and their associated strong shaking [e.g., Geller et al., 1997; Silver, 1998]. This is partially due to a high susceptibility of critically stressed faults to transient loading or external stress perturbation, as well as our inability to measure absolute stress and failure strength at depths where most ruptures nucleate.

It is widely accepted that dynamic stress change from passing seismic waves can trigger local seismic activity at regional and teleseismic distances (typically more than 5 times the mainshock rupture length), where the Coulomb stress changes due to static fault displacement are negligible [Hill and Prejean, 2015, and references therein]. Dynamically triggered events during or immediately following distant mainshocks can be easily recognized due to their temporal coincidence with the triggering seismic waves. They can commonly be explained with a simple Coulomb failure criterion model in which dynamic stress plus in-situ shear stress acting on a fault close to failure are larger than the fault strength [Hill, 2012]. In comparison, events can also occur long after the passage of seismic waves, and secondary triggering mechanisms (e.g., movement of fluids, aseismic slip) have been invoked to explain delayed triggering phenomena [Parsons, 2005; Shelly et al., 2011; Parsons et al., 2017]. Understanding the interaction between the passing seismic waves and critically stressed faults could shed light on the nucleation process of earthquakes, and eventually increase our ability to forecast future occurrence of large damaging earthquakes [Brodsky and van der Elst, 2014] by improving our understanding of the spatially-heterogeneous nature of time-dependent seismic hazard.

* Corresponding author.
E-mail address: dongdony@umich.edu (D. Yao).

https://doi.org/10.1016/j.epsl.2020.116723
0012-821X/

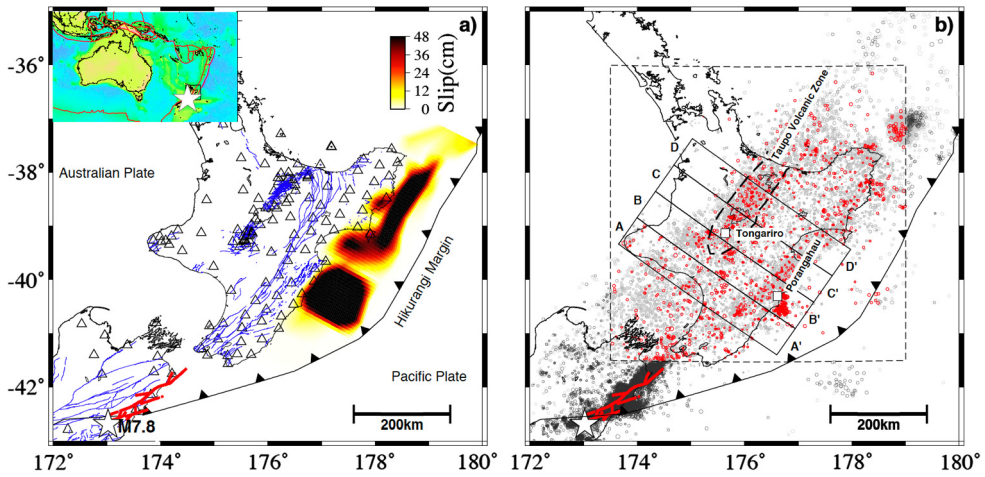

Fig. 1. Map of the study region. a) Solid blue curves show mapped faults. Open triangles are seismic stations. Slip distribution during the triggered shallow SSE is adopted from Wallace et al. (2017). Left top insert shows the study region in a bigger context. b) Events from GeoNet from 2016/03/01 to 2017/03/01 are shown with gray circles within dashed box, while red circles are used template earthquakes in this study. Black circles are catalog events outside dashed box since Kaikōura mainshock till 2017/03/17. Cross-sections AA', BB', CC' and DD' are plotted in Fig. 2. Regions highlighted include the Taupo Volcanic Zone (TVZ), Mt. Tongariro, as well as Porangahua coast. (For interpretation of the colors in the figure(s), the reader is referred to the web version of this article.)

Earthquake triggerability could be affected by many factors, including the characteristics of stress perturbations (as a function of fault orientation, amplitude and incident angle of incoming seismic wave, etc.) and background stress state of the triggered fault system [van der Elst and Brodsky, 2010]. While triggered earthquakes have been observed in many different tectonic settings [Hill and Prejean, 2015], they mostly occur in extensional or transextensional regions (such as volcanic or geothermal areas). Those regions are normally characterized as seismically active with abundant presences of pore fluids [Hill and Prejean, 2015]. Empirical observations have shown that dynamic stress perturbation on the order of a few to tens of kilopascals are capable of triggering earthquakes [Brodsky and Prejean, 2005].

The M_w 7.8 Kaikōura earthquake struck the South Island of New Zealand at 12:03 am local time on November 14th, 2016 (2016/11/13 11:02:56.35 UTC). The mainshock epicenter located near the transition from the Hikurangi subduction zone to the Northeast to the transpressional Alpine fault plate boundary to the Southwest (Fig. 1). The earthquake ruptured multiple active faults with surface slip up to 10 m and terminated offshore near the Cook Strait [Hamling et al., 2017; Kaiser et al., 2017]. The earthquake triggered several shallow slow slip events (SSE) in the North Island [Wallace et al., 2017], and possible deep slip events [Wallace et al., 2018]. The majority of slow slip occurred along the shallow portion of the Hikurangi subduction interface near the Hawke's Bay (Fig. 1). Wallace et al. (2017) and Kaneko et al. (2019) suggested that the low-velocity sedimentary wedge likely acted as an amplifier, together with the rupture directivity, to promote dynamic triggering of shallow slow-slip events.

Peng et al. (2018) reported triggered microearthquakes and tremor in both islands following the Kaikōura mainshock. Using earthquakes listed in the GeoNet catalog, they found several regions with clear evidence of dynamically triggered earthquakes in the North Island. However, they also suggested that the reported observations could be incomplete due to potential bias from missing events that embedded in the coda of the mainshock and large aftershock. Our study is an extension of that work. Specifically, we obtained a more complete catalog of earthquakes in the North Island by using a waveform matched filter technique (WMFT). We compared the seismicity rate change pattern with the dynamic stress change using two kinematic source models [Holden et al., 2017; Wang et al., 2018], in order to better understand how different tectonic environments respond to the stress perturbations.

2. Study region

The tectonic setting of New Zealand is rather complex. In the South Island, the oblique strike-slip Alpine fault connects the westward dipping Hikurangi subduction zone and the eastward dipping Puysegur subduction zone, forming the current tectonic framework around which convergence of the Australian and Pacific plates is accommodated (Fig. 1). In the North Island, the Pacific plate subducts obliquely beneath the Australian plate along the Hikurangi margin with slip rates of 39-48 mm/yr [Beavan et al., 2016]. This convergence drives back-arc rifting and volcanism in the Taupo Volcanic Zone (TVZ), which has been active for the past two million years, including recent eruptions of Mt. Ruapehu [e.g. Jolly et al., 2010] and the Tongariro volcano [e.g. Hurst et al., 2014]. Earthquake swarms and volcanic tremors occur frequently in these regions, and are actively monitored by seismic stations in the GeoNet. Near the southern end of the North Island, westward plate convergence is partitioned into trench-normal motion on the subduction zone and trench-parallel motion in upper plate strike-slip faults [Nicol and Beavan, 2003], while the forearc rotates with increasing subduction rate farther to the north near the Havre Trough [Wallace et al., 2004]. Hence, background seismicity in the North Island is typically associated with the Hikurangi subduction zone, magma movements within the TVZ, or tectonic movements in the upper crustal faults.

In addition to regular earthquakes, dozens of slow slip events have been detected and characterized in the North Island [e.g., Wallace and Beavan, 2010; Wallace et al., 2012]. These slow slip events comprise shallow and frequent (∼every 1-2 years) and deeper infrequent (∼ every 5 years) events. In the Gisborne and Hawke's Bay regions, the shallow (<15 km depth) slow slip events occur around every two years and last for about two weeks each. Beneath the Manawatu and Kapiti regions, deeper (25-60 km depth) slow slip events can last over one year.

3. Data and method

We selected 1,713 earthquakes between 2016/11/01 and 2016/11/30 in the GeoNet catalog as candidate template events (Table S1; last retrieved on September 2020; Fig. 1) and used the WMFT to search for events with similar waveforms in continuous data to obtain a more complete catalog in the North Island around the mainshock. Fig. 2 shows four cross-sections of the interface geometry for the Hikurangi subduction zone [Williams et al., 2013],

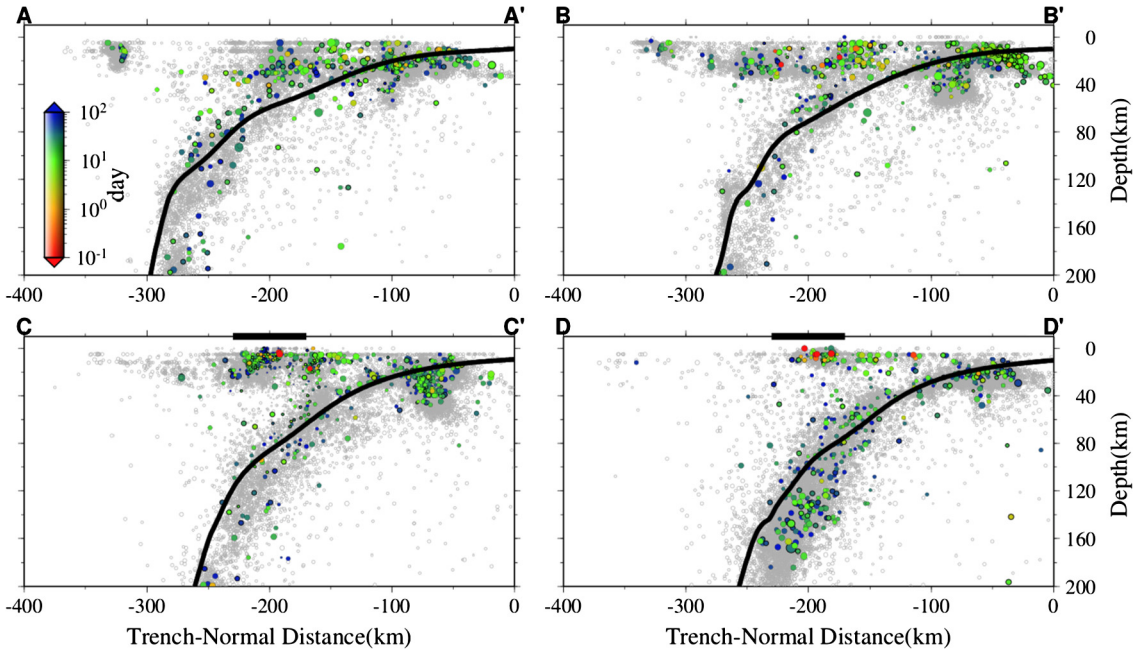

Fig. 2. Depth profiles along the marked cross-sections in Fig. 1. Events after the Kaikōura mainshock are color-coded with the elapsed time. Open gray circles are earthquakes before the mainshock since 2010. Bold black curves show the Pacific plate geometry from Williams et al. (2013). The horizontal bars along section CC' and DD' outline the projected TVZ.

together with seismicity listed in the GeoNet catalog from 2010/01 to 2020/09. Events within first 3 months following the Kaikōura mainshock within our study region are color-coded by the elapsed time since the mainshock, highlighting regions with potential seismicity rate increases following the mainshock [Peng et al., 2018].

Continuous waveforms from 2016/11/01 to 2016/11/30 (both HH and EH components) for all nearby stations within the North Island (Fig. 1) were requested via the CWB client from GeoNet (https://www.geonet.org.nz/data/tools/CWB; Last accessed March 2017). We applied a 5-15 Hz band-pass filter on the continuous data to suppress possible contamination from distant sources (especially energy below 5 Hz from the mainshock and its aftershock zone; Fig. S1) and to increase the relative strength of local earthquake signals. To reduce computational cost, we down-sampled the original waveform with 100 samples per second (sps) for HH and 100 or 200 sps for EH to a uniform 40 sps.

Waveforms of stations within 150 km relative to each template event were cut from filtered and down-sampled continuous data, and phase picks using GeoNet FDSN Event webservice were saved (http://geonet.org.nz/data/tools/FDSN). Due to the inclusion of automatic phase picks and event association with 1D velocity model, some catalogued events might be still mislocated (Fig. S2) or contain no robust phase picks [Yao, 2018]. Hence, we carefully examined phase picks for all 1,713 events and removed badly assigned phase picks. To avoid noisy traces, we computed the signal to noise ratio (SNR) for each trace, which was defined as the ratio between the cumulative energy of the signal window (the same window used for detection: a 5s-long window starting 1 s before the P and S arrivals for vertical and horizontal components, respectively) and noise window (a 5s-long window ending 1 s before the P arrival). Eventually, 1,466 events containing at least 9 channels with SNR above 5 were used as templates.

For each template trace, we used the above defined signal window to run a sliding window cross-correlation (CC) with the corresponding continuous trace and obtain a single CC function. After shifting back to the template's origin time based on the arrival time, all CC functions of a common template were stacked together to generate an average daily trace. We registered a positive detection when the mean stacked CC value is above a pre-defined threshold. This was generally defined as the median CC of the stacked daily trace plus a scaled multiple of its Median Absolute Deviation (MAD) [Shelly et al., 2007]. After combining detections from all templates, we removed duplicate ones by keeping the one with largest CC value every 3 s. We further cross-correlated events with origin time separated by less than 30 s using the above used signal window, and allowed a maximum of 0.5 s time shift. The one with largest MAD was kept when two or more events have nearly identical waveform. The magnitudes of newly detected events were computed based on the median peak amplitude ratios relative to best-matching templates with the highest CC value [Peng and Zhao, 2009]. Since only nearby events can be matched with high CC values and we focused on the overall patterns of seismicity rate changes, assigning the location of best-matching template to the newly detected event meet the scope of our current study.

4. Results

4.1. Event detection results

The detection with 1,466 catalog events as templates resulted in ~10,830 and ~6,050 additional events within the one-month study period above the 9 and 12 times MAD threshold (Tables S2 and S3). These catalogs have ~7 and 4 times more events compared to those in the GeoNet catalog during the one-month period. Fig. 3 shows an example of M_L 1.79 and M_L 2.03 earthquakes that occurred at 2016/11/16 17:44:08 and 2016/11/16 17:44:19 UTC (~11 s apart). Both were matched by a M_L 3.1 template event 2016p867469 (origin time: 2016/11/16 23:07:37.68 UTC) with mean CC values of 0.73 and 0.72, which are about 60 times MAD, well above the threshold. The cumulative frequency-magnitude distribution for the GeoNet and detected catalogs are plotted in Fig. S3, and the corresponding magnitudes of completeness (Mc) from the best-combined method [Wiemer, 2001] are 2.1 and 1.8, respectively.

The detection result provides a better image of seismicity distribution in the North Island (Fig. 4a): the TVZ is mostly characterized with shallow crustal earthquakes (<10 km) and shows

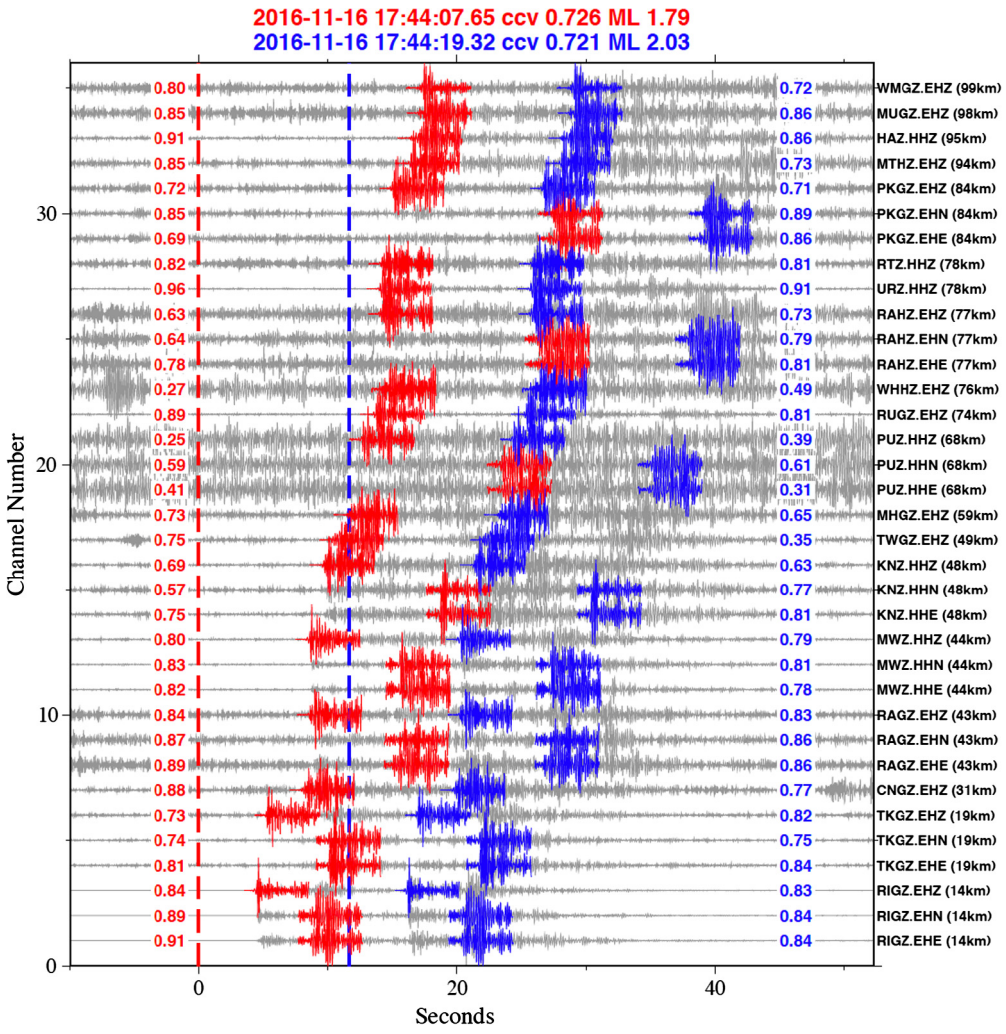

Fig. 3. An example showing two newly detected earthquakes by the WMFT. Gray waveforms show continuous traces (the origin time corresponds to 2016/11/16 17:44:07.65 UTC), sorted by the epicentral distance (labeled on the right side) relative to the template. Red and blue waveforms are template waveform (GeoNet id: 2016p867469, M_L 3.1 with origin time 2016/11/16 23:07:37.68 UTC) used in cross-correlation (CC). CC values on each trace for both new events are marked, and the new event information is labeled on top.

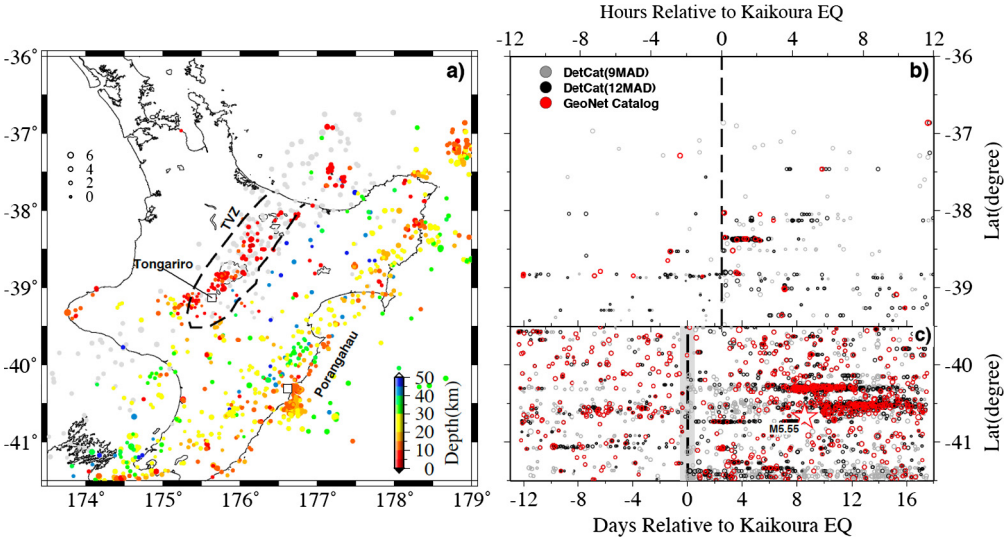

Fig. 4. Earthquake detection result. a) the spatial distribution of all events in the detected catalog (9MAD), color-coded by the GeoNet's hypocentral depth. b) Latitude versus time for events in the detected catalog emphasizing the TVZ 12 hours before and after the Kaikōura mainshock (marked by the vertical dashed line): 9MAD (gray), 12MAD (black), as well as GeoNet catalog (red). c) seismicity within the detection window (13 days before and 18 days after). The M_L 5.55 earthquake near Porangahua coast is labeled.

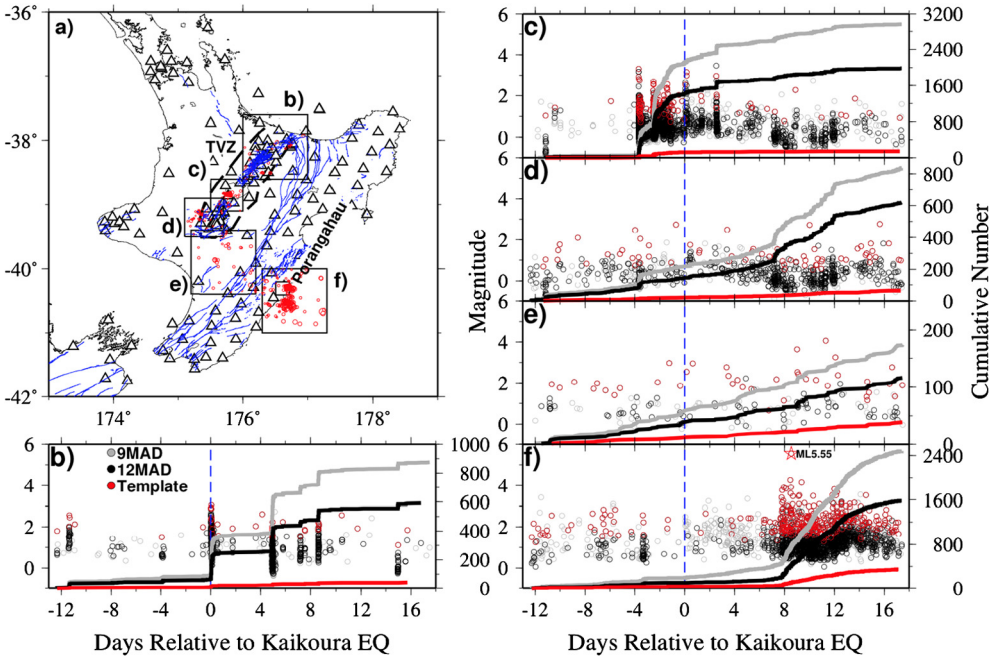

Fig. 5. Detection result within highlighted regions; b), c) and d) are around the TVZ, e) south to the Tongariro volcano, f) Porangahau coast. Detected events above 9MAD and 12MAD are shown with gray and black circles, while template events are marked with red circles. The corresponding cumulative number of earthquakes are plotted with solid line of same color.

short-term increase right after the mainshock (Fig. 4b), while the east coast exhibits active occurrence of earthquakes along the plate interface (10-20 km) with a ~8 days delay (Fig. 4c).

We further highlight several regions: surrounding the TVZ (Fig. 5b, 5c & 5d), immediately south of Tongariro volcano (Fig. 5e) and near the Porangahau on east coast (Fig. 5f). To avoid potential bias of using a simple pre-defined threshold, we plot events and cumulative numbers with both 9MAD and 12MAD thresholds and catalog events. A moderately elevated seismicity within TVZ in the short time window can be found, especially north of Lake Taupo (Fig. 5b), which was also revealed by our recent analysis with the GeoNet catalog [Peng et al., 2018]. Within Lake Taupo, although an active earthquake swarm started ~4 days before the Kaikōura earthquakes, both visual inspection and the newly detected catalog reveal instantaneously triggered earthquake within and immediately the passing surface waves (Fig. S1; Peng et al. (2018); Fig. 4b). The seismicity in a region near the Porangahau coast started to increase after one week following the mainshock, where a delayed slow-slip event has been triggered by the Kaikōura mainshock [Wallace et al., 2017; Peng et al., 2018].

4.2. Seismicity rate change

To further quantify seismicity rate change for both template-matching catalogs, we compared the observed number of earthquakes within the target time period to the predicted value based on its background rate, which is termed as the β value [Matthews and Reasenberg, 1988; Aron and Hardebeck, 2009]. Specifically, the background window was defined as a 300-hour (12.5 day) window starting from 11/01/2016 (starting time of the detection) to the mainshock occurrence time. A β value for each 0.05° by 0.05° grid was computed by comparing the observed number of earthquakes within the "triggered" window with the predicted values and normalized by the standard deviation as

$$\beta = \frac{N_a - N\,(T_a/T)}{\sqrt{N\,(T_a/T)\,(1 - T_a/T)}} \quad (1)$$

where N_a is number of earthquakes within the "triggered" window of length T_a. N is the total earthquake number for the entire window of which the duration is T, containing both "background" T_b and "triggered" T_a windows. Statistically, a β value above 2 indicates a significant seismicity rate increase, while a significant decrease occurs when β value is below -2 [Hill and Prejean, 2015]. Minor to no statistically significant changes exist when β value is between -2 and 2.

We used different T_a windows after the mainshock in order to quantify both instantaneous/short-term and delayed/long-term triggering effects: the first was within 1 day following the mainshock, and the second was from the mainshock to the end of detection window (17.5 days). The β map of the above two triggered windows for the detection (9MAD) is shown in Fig. 6: a) and c) are results for GeoNet catalog events, while b) and d) are corresponding panels for the newly detected catalog. Since the Mc generally changes with time, especially right after the occurrence of a mainshock. We followed the approach from Hainzl (2016) to measure time-dependent Mc(t). We further selected events with M > Mc(t) to define β statistics (Fig. S4). The detected catalogs show an obvious change of seismicity within the TVZ with the short-term window, and around the Porangahau coast with the long-term window. Similar figures for the detection result above 12MAD can be found in Fig. S5.

4.3. Comparison with dynamic stress

We then used the same method as described in Wallace et al. (2017) to compute dynamic stress changes in the period range of 3 and 100 seconds. The only difference was that here we used both the updated kinematic source model in Holden et al. (2017) (based on local strong-motion and geodetic data, hereafter termed the *Holden's Model*) and Wang et al. (2018) (which includes ~45% of the total moment release from the Hikurangi subduction interface, hereafter termed the *Wang's Model*). At each point in the crust, stress tensor time-series were computed and converted into the time-series of the square root of the second invariant of the deviatoric stress tensor, sqrt(J_2). Fig. 7 shows max(sqrt(J_2)) at both

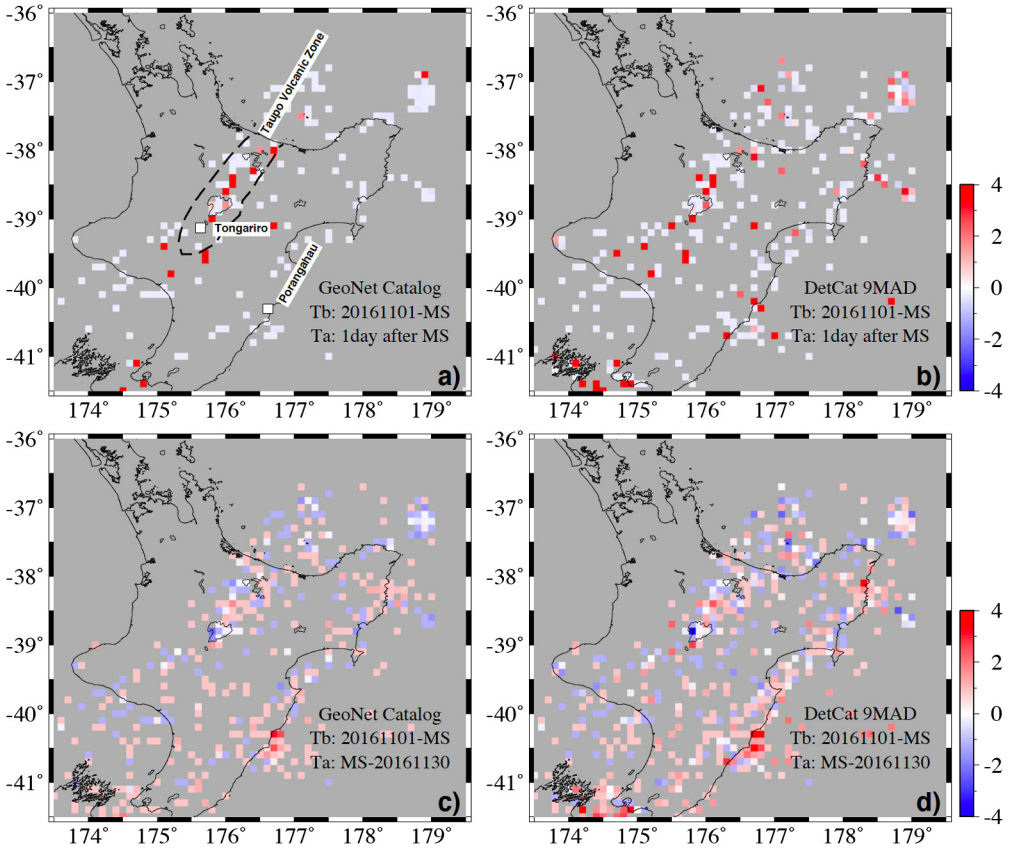

Fig. 6. Beta map for the template and detected catalog (9MAD), with time-depended Mc(t) applied. a) and b): short-term change using 1day after the mainshock as the "triggered window". c) and d): long-term change using mainshock to the end of Nov (~17.5 days) as the "triggered window". Gray shaded area are grids without catalog earthquakes.

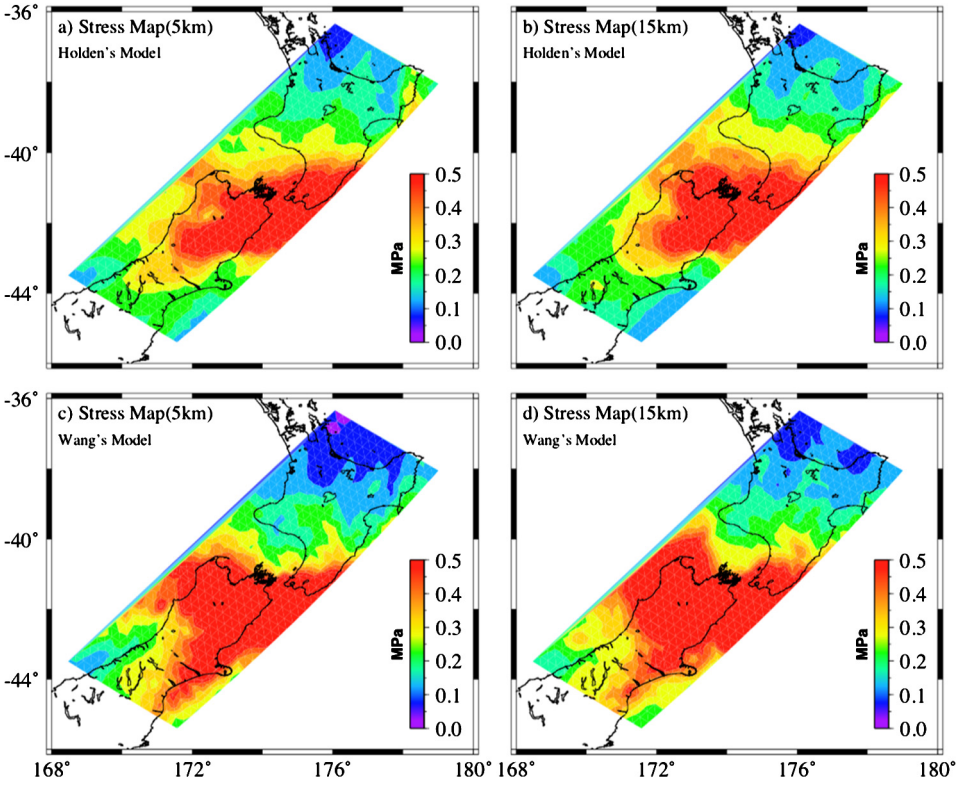

Fig. 7. Dynamic stress changes, max(sqrt(J_2)), in the period range of 3 and 100 seconds at two depths (5 km and 15 km) from both the updated kinetic source model (*Holden's* and *Wang's model*).

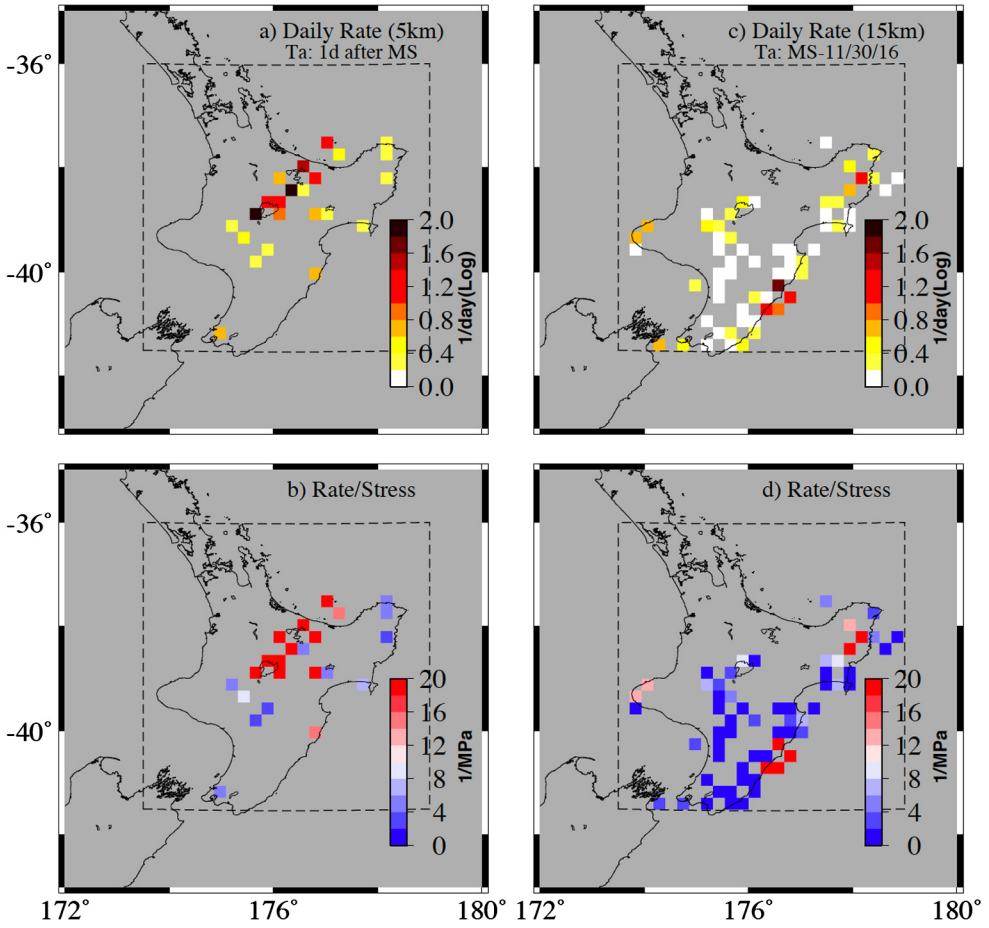

Fig. 8. Comparison between the daily seismicity rate for the detection (9MAD) and calculated dynamic stress (*Holden's Model*). a) and c) show the daily seismicity rate in short "triggered window" at shallow depth (0-10 km) range, and long "triggered window" within depth range of 10-20 km. b) and d) indicate the defined dynamic stress "susceptibility".

5 km and 15 km depths, which correspond to shallow seismicity within TVZ and those along the subducting interface near the Porangahau coast.

Next we computed the daily seismicity rate during the two triggered windows at different depth ranges (Fig. 8a, 8c). Considering large depth uncertainty, we used a depth range of 0-10 km for instantaneously triggered shallow events within TVZ, and 10-20 km for delayed triggered earthquake clusters near the subduction zone by the Porangahau coast (Fig. 2). Following Brenguier et al. (2014), we defined the dynamic stress "susceptibility" as the ratio between the observed daily seismicity rate and the maximum amplitude of estimated dynamic stress changes, max(sqrt(J_2)). We reported dynamic stress susceptibility at depth slices of 5 km and 15 km, representing seismicity around the shallow crust in the TVZ and Hikurangi subduction interface, respectively. The corresponding "susceptibility" maps using dynamic stress change based on the *Holden's Model* for the detection (9MAD) with both short and long-term windows are shown in Fig. 8b and 8d. Results based on detections above 12MAD as well as using the *Wang's Model* can be found in Figs. S6-S8. As expected, for the short-term window, regions around and to the south and east of the TVZ are highlighted. For the long-term window, regions along the east coast, and isolated regions around the TVZ are highlighted.

5. Discussions

In this study we performed systematic event detections in North Island following the 2016 M_w 7.8 Kaikōura earthquake, and found clear evidence of triggered earthquakes in the North Island at multiple spatial-temporal windows. Because the waveform matching technique strongly depends on the reliability of the template catalog, the inclusions of mislocated templates could introduce additional false detections, resulting in possible erroneous interpretation [e.g., Yao, 2018]. Hence, before discussing potential mechanisms and implications of our results, we checked the quality of our newly detected events.

5.1. Visual inspection of the newly detected events

We first examined the 5-15 Hz bandpass filtered waveform for stations around the TVZ to demonstrate that our analysis can help uncover missing smaller events triggered by passing seismic waves of the mainshock. As shown in Fig. S9, many previously missing events were detected by our method, while only 2 were listed in the GeoNet catalog. In the detection of 9MAD, a total number of 32 events occurred in the first 1200 s and 6 out of 30 missed events are above the time-dependent Mc (∼3). In comparison, the detection of 12MAD contains 16 events in the first 1200 s, and 3 out of 14 are above Mc (∼2.5). However, some events were still not detected by our method. It is possible that some earlier triggered events were tremor with longer duration and no clear phase arrivals [Peng et al., 2018], and hence cannot be matched by earthquake templates. In addition, some missing earthquakes could occur in regions that were not active immediately before or after the mainshock. Hence, we might not have the right template event to match them.

We further showed waveforms of the first 100 events in both detection catalog (see Supplementary Material). For each detected

event, we only plotted out waveforms for selected channels on which the best-matched template (i.e., the template that has the highest mean CC value when multiple templates match the detect event) has SNRs above 5. In order to make a direct comparison, the corresponding template waveforms were also plotted. While some of the newly detected events can be visually identified, others cannot, raising the question on whether these events are real earthquakes or not.

It is worth noting that the advantage of the network-based WMFT is to enhance weak but consistent signals when multiple channels were stacked. For instance, Li et al. (2015) showed that when stacking with plenty of stations, the method could possibly detect a seismic event that is completely buried in the background noise. To verify this, here we also designed a simple test. We selected a M_L 2.1 earthquake in the GeoNet catalog (2016p834777: 2016/11/04 20:49:20), and gradually reduced its amplitude by multiplying 10^(−0.1), 10^(−0.2), ..., until 10^(−3). These events with reduced amplitudes were added on top of continuous waveforms of the day 2016/11/04 before the catalog event's origin time with a time step of 300 s (Fig. S10). We then used the M_L 2.1 template to scan the continuous waveforms on the day 2016/11/04, and saved positive detections above the 9MAD threshold. As expected, the MFT can still detect the buried signal with amplitude lower than the seismic noise, and the noise level in the stacked correlation trace is significantly reduced by adding more stations/channels. Shelly et al. (2007) also performed similar analysis to justify the robustness of their low-frequency earthquake detection in southwest Japan. Hence, while we could not independently verify that all the new detections were real events, we should not reject them simply because they were below the background noise level (and hence cannot be visually confirmed).

5.2. Bias from automatic mislocated catalog events

A relatively less constrained region is immediate to the south of TVZ, where an elevated seismicity was noted by Peng et al. (2018) with β values well above 2. This region is away from any mapped active faults or volcanoes. There are a few close-by stations (Fig. 1), which might result in poorly constrained event locations, especially in the automatically generated catalogs without human analysts' review, which was used in Peng et al. (2018).

By manually inspecting the waveforms, we found that many events along the extended band to the south of TVZ are either mislocated, or their phase arrivals are falsely picked. The potential causes include contaminated energy from the mainshock and aftershock zone at the lower frequency range (Fig. S1), as well as badly constrained locations using only P phases or erroneously labeled phases (Fig. S2). We found that phase picks used for these events were mostly P arrivals from an automatic Short-Term Average/Long-Term Average (STA/LTA) algorithm, while additional manually picked arrivals help resolve better locations for other kept catalog events. This was further confirmed by the most recent GeoNet catalog used in this study (last retrieved on 09/2020). As shown in Fig. S11, most of the events in this region right after the Kaikōura mainshock were removed by subsequent manual phase picks and relocations.

The inclusions of those templates could result in a biased increase of local seismicity within the region to the south of TVZ [Yao, 2018], which was already evident in the GeoNet data alone (Fig. 3 in [Peng et al., 2018]). By filtering out lower-frequency energies and adjusting their phase picks and locations manually, we could remove the biased observation to some degree. These mislocated events can only be resolved by carefully examining the phase picks and relocating using updated velocity models, which requires additional analysts' efforts.

5.3. Triggering mechanism

In Section 4.3, we made direct comparisons between the calculated dynamic stress and resulting seismic rate with different time scales in order to better distinguish different triggering phenomena at different locations. As mentioned before, volcanic or geothermal areas are susceptible to external stress perturbations, likely to due to the existence of excessive fluids and critically stressed faults and volcanic systems [Brodsky and Prejean, 2005]. These sites generally respond to transient dynamic stress loading instantaneously, and the triggered seismicity decays quickly with time since the passage of seismic waves, likely following an Omori's law-type decay [Brodsky, 2006; Meng and Peng, 2014]. Near the volcanic/geothermal site within the TVZ, Peng et al. (2018) found four regions of instantaneously triggered earthquakes/tremor during the surface waves. In this study, we also found moderate to significant seismicity rate increase immediately following the Kaikōura mainshock (Figs. 4 and 5), but the rate changes quickly returned back to the background levels. In comparison, the seismicity rate changes lasted longer near the east coast (Figs. 4 and 5), where triggered SSEs had been observed [Wallace et al., 2017].

The occurrence of dynamically triggered SSE, together with earthquake cluster, provide important clues on the earthquake nucleation process and how the shallow megathrust releases the accumulated strain. As mentioned before, the Hikurangi margin along the Gisborne in the North to Hawkes' Bay farther south experiences regular occurrence of shallow SSEs in the past decade together with elevated earthquake rates [e.g., Wallace and Beavan, 2010; Wallace et al., 2012; Delahaye et al., 2009; Todd et al., 2018], indicating weak coupling at shallow depths between the Pacific and the Australian Plates. Wallace et al. (2017) and Kaneko et al. (2019) reported the enhanced occurrence of several SSEs in the shallow Hikurangi subduction zone, likely due to propagation and trapping of large amplitude seismic waves along the shallow trench. This is similar to the observation of triggered shallow SSEs near Boso Peninsula, Japan following the 2011 M9.1 Tohoku-Oki earthquake [Hirose et al., 2012] and of shallow SSEs triggered by several regional earthquakes in Nankai Trough [Araki et al., 2017; Katakami et al., 2020]. In many cases, SSEs are accompanied by the occurrence of earthquake clusters.

The interaction among dynamic stress perturbation, SSE/creep and accompanied earthquakes/tremors was proposed as an alternative mechanism for delayed triggering [e.g., Kanamori, 2008; Shelly et al., 2011, etc.]. Specifically, an SSE could be initiated by an external stress perturbation, which takes time to unfold itself. The SSE could either drive/generate nearly continuous tremor signals at depth, or microearthquakes at shallow depth. The resulting seismic sources typically migrate in the similar way as the SSE evolves spatially. Sometimes the ongoing SSE could load a nearby locked patch to failure, resulting in larger damaging earthquakes [Kato et al., 2012]. To further characterize this, Kaneko et al. (2018) developed a simple method to include the impact of SSEs on triggering megathrust earthquakes. More comprehensive earthquake catalogs, such as the one we developed in this study, may be useful to infer regions of enhanced stress on plate interface due to SSEs and evaluate the potential for the occurrence of a subsequent megathrust earthquake.

We note that the broad region sandwiched between the TVZ and Porangahau did not experience any obvious change of seismicity following the mainshock (Fig. 8), which is geographically closer to the mainshock rupture and in the right direction of the rupture directivity effects. Given the spatially varying Mc and elevated level after the mainshock [Harte, 2019], the observation of triggering in this region could be limited. Additionally, one candidate explanation is this region locates within the static stress shadow. However, the static stress change model shows slightly positive value on

crustal faults in the southwestern North Island (I. Hamling, personal communication; [Xu et al., 2018]), which should promote the occurrence of local earthquakes. Another possible explanation might be the quiescence since the last deep SSE (later 2014 until early 2016) around Manawatu [Wallace and Beavan, 2010], which is consistent with the observation that no dynamically-triggered SSE following the Kaikōura mainshock has been reported near Manawatu.

6. Conclusion

We performed a systematic detection of microseismicity in the North Island of New Zealand following the 2016 Kaikōura mainshock. About 4-7 times more events than listed in the GeoNet catalog have been detected, showing significant seismicity rate increase as a function of location and time. Specifically, small earthquakes in several regions within the TVZ were instantaneously triggered by moderate dynamic stress changes from the mainshock, but the seismicity rate changes were short-lived. On the other hand, the Hikurangi subduction zone showed increase of seismicity day to weeks later, likely to be driven by the triggered SSEs. In addition, we showed that a clean template event database is critical to ensure the quality of the subsequent template matching results and interpretation. Our result suggests that large earthquakes in the magnitude 7-8 ranges are capable of triggering fault slip and affecting seismicity patterns at regional distances of a few hundred kilometers (beyond the traditional aftershock zones). This may pose additional seismic hazards in regions that are critically stressed.

CRediT authorship contribution statement

Dongdong Yao: Conceptualization, Data curation, Formal analysis, Investigation, Methodology, Visualization, Writing – original draft, Writing – review & editing. **Zhigang Peng:** Conceptualization, Funding acquisition, Methodology, Project administration, Supervision, Validation, Writing – review & editing. **Yoshihiro Kaneko:** Conceptualization, Formal analysis, Methodology, Writing – review & editing. **Bill Fry:** Conceptualization, Funding acquisition, Validation, Writing – review & editing. **Xiaofeng Meng:** Formal analysis, Methodology, Writing – review & editing.

Declaration of competing interest

The authors declare that they have no known competing financial interests or personal relationships that could have appeared to influence the work reported in this paper.

Acknowledgement

All of the seismological data used in this study are archived at GeoNet (https://www.geonet.org.nz/data). We thank Ian Hamling and Laura Wallace for sharing the digital surface rupture trace of the 2016 Kaikōura mainshock, and the inverted slip distribution of the triggered SSEs. The seismic data are processed with SAC and GMT tools. ZP and DY are supported by National Science Foundation Grants EAR-1725165 and EAR-1818611. ZP acknowledges additional support from Georgia Tech College of Science's Faculty Development Grant. This work used the Extreme Science and Engineering Discovery Environment (XSEDE, Towns et al., 2014) Stampede2 at the Texas Advanced Computing Center (TACC) through allocation TG-MCA03S012. XSEDE is supported by National Science Foundation grant number ACI-1548562. Numerical simulations for computing dynamic stress changes were run on the New Zealand eScience Infrastructure (NeSI) high-performance computing facilities.

Appendix A. Supplementary material

Supplementary material related to this article can be found online at https://doi.org/10.1016/j.epsl.2020.116723.

References

Araki, E., Saffer, D.M., Kopf, A.J., Wallace, L.M., Kimura, T., Machida, Y., 2017. I.O.D.P. Expedition. Recurring and triggered slow-slip events near the trench at the Nankai Trough subduction megathrust. Science 356 (6343), 1157–1160.

Aron, A., Hardebeck, J.L., 2009. Seismicity rate changes along the central California coast due to stress changes from the 2003 M 6.5 San Simeon and 2004 M 6.0 Parkfield earthquakes. Bull. Seismol. Soc. Am. 99, 2280–2292. https://doi.org/10.1785/0120080239.

Beavan, J., Wallace, L.M., Palmer, N., Denys, P., Ellis, S., Fournier, N., Hreinsdottir, S., Pearson, C., Denham, M., 2016. New Zealand GPS velocity field: 1995–2013. N.Z. J. Geol. Geophys. 59, 5–14. https://doi.org/10.1080/00288306.2015.1112817.

Brenguier, F., Campillo, M., Takeda, T., Aoki, Y., Shapiro, N.M., Briand, X., Emoto, K., Miyake, H., 2014. Mapping pressurized volcanic fluids from induced crustal seismic velocity drops. Science 345 (6192), 80–82.

Brodsky, E.E., Prejean, S.G., 2005. New constraints on mechanisms of remotely triggered seismicity at Long Valley Caldera. J. Geophys. Res. 110, B04302. https://doi.org/10.1029/2004JB003211.

Brodsky, E.E., 2006. Long-range triggered earthquakes that continue after the wave train passes. Geophys. Res. Lett. 33 (15).

Brodsky, E.E., Van der Elst, N.J., 2014. The uses of dynamic earthquake triggering. Annu. Rev. Earth Planet. Sci. 42, 317–339. https://doi.org/10.1146/annurev-earth-060313-054648.

Delahaye, E.J., Townend, J., Reyners, M.E., Rogers, G., 2009. Microseismicity but no tremor accompanying slow slip in the Hikurangi subduction zone, New Zealand. Earth Planet. Sci. Lett. 227 (1–2), 21–28.

Geller, R.J., Jackson, D.D., Kagan, Y.Y., Mulargia, F., 1997. Earthquakes cannot be predicted. Science 275, 1616.

Hainzl, S., 2016. Rate-dependent incompleteness of earthquake catalogs. Seismol. Res. Lett. 87 (2A), 337–344. https://doi.org/10.1785/0220150211.

Hamling, I., Hreinsdóttir, S., Clark, K., Elliott, J., Liang, C., Fielding, E.J., Litchfield, N., Villamor, P., Wallace, L., Wright, T.J., D'Anastasio, E., Bannister, S., Burbridge, D., Denys, P., Gentle, P., Howarth, J., Mueller, C., Palmer, N., Pearson, C., Power, W., Barnes, P., Barrell, D., Van Dissen, R., Langridge, R., Little, T., Nicol, A., Pettinga, J., Rowland, J., Stirling, M., 2017. Complex multi-fault rupture during the 2016 M_w 7.8 Kaikōura earthquake, New Zealand. Science. https://doi.org/10.1126/science.aam7194.

Harte, D.S., 2019. Evaluation of earthquake stochastic models based on their real-time forecasts: a case study of Kaikoura 2016. Geophys. J. Int. 217 (3), 1894–1914.

Hill, D.P., 2012. Dynamic stresses, Coulomb failure, and remote triggering-corrected. Bull. Seismol. Soc. Am. 102, 2313–2336.

Hill, D.P., Prejean, S.G., 2015. Dynamic triggering. In: Schubert, G. (Ed.), Treatise on Geophysics, 2nd edition. Elsevier, Amsterdam. Chapter 8 in Volume 4, "Earthquake Seismology" H. Kanamori (Ed.).

Hirose, H., Kimura, H., Enescu, B., Aoi, S., 2012. Recurrent slow slip event likely hastened by the 2011 Tohoku earthquake. Proc. Natl. Acad. Sci. USA 109 (38), 15157–15161.

Holden, C., Kaneko, Y., D'Anastasio, E., Benites, R., Fry, B., Hamling, I.J., 2017. The 2016 Kaikōura earthquake revealed by kinematic source inversion and seismic wavefield simulations: slow rupture propagation on a geometrically complex crustal fault network. Geophys. Res. Lett. 44, 11,320–11,328. https://doi.org/10.1002/2017GL075301.

Hurst, T., Jolly, A.D., Sherburn, S., 2014. Precursory characteristics of the seismicity before the 6 August 2012 eruption of Tongariro volcano, North Island, New Zealand. J. Volcanol. Geotherm. Res. 286, 294–302. https://doi.org/10.1016/j.jvolgeores.2014.03.004.

Jolly, A.D., Sherburn, S., Jousset, P., Kilgour, G., 2010. Eruption source processes derived from seismic and acoustic observations of the 25 September 2007 Ruapehu eruption North Island, New Zealand. J. Volcanol. Geotherm. Res. 191 (1), 33–45.

Kaiser, A.E., Balfour, N., Fry, B., Holden, C., Litchfield, N., Gerstenberger, M., D'Anastasio, E., Horspool, N., McVerry, G., Ristau, J., Gledhill, K., Bannister, S., Christopherson, A., Clark, K., Power, W., Rhoades, D., Hamling, I., Wallace, L., Mountjoy, J., Kaneko, Y., Benites, R.A., Van Houtte, C., Massey, C., Dellow, S., Hreinsdottir, S., 2017. The 2016 Kaikōura (New Zealand) earthquake: preliminary seismological report. Seismol. Res. Lett. 88 (3). https://doi.org/10.1785/0220170018.

Kanamori, H., 2008. Earthquake physics and real-time seismology. Nature 451, 271–273.

Kaneko, Y., Wallace, L.M., Hamling, I.J., Gerstenberger, M.C., 2018. Simple physical model for the probability of a subduction-zone earthquake following slow slip events and earthquakes: application to the Hikurangi megathrust, New Zealand. Geophys. Res. Lett. 45, 3932–3941. https://doi.org/10.1029/2018GL077641.

Kaneko, Y., Ito, Y., Chow, B., Wallace, L.M., Tape, C., Grapenthin, R., D'Anastasio, E., Hino, R., Henrys, S., 2019. Ultra-long duration of seismic ground motion arising from a thick, low-velocity sedimentary wedge. J. Geophys. Res. 124 (10), 1–13. https://doi.org/10.1029/2019JB017795.

Katakami, S., Kaneko, Y., Ito, Y., Araki, E., 2020. Stress sensitivity of instantaneous dynamic triggering of shallow slow slip events. J. Geophys. Res. 125. https://doi.org/10.1029/2019JB019178.

Kato, A., Obara, K., Igarashi, T., Tsuruoka, H., Nakagawa, S., Hirata, N., 2012. Propagation of slow slip leading up to the 2011 M_w 9.0 Tohoku-Oki earthquake. Science 335, 705–708.

Li, Z., Peng, Z., Meng, X., Inbal, A., Xie, Y., Hollis, D., Ampuero, J.P., 2015. Matched filter detection of microseismicity in Long Beach with a 5200-station dense array. In: 2015 SEG Annual Meeting. New Orleans, Louisiana, pp. 2615–2619.

Matthews, M.V., Reasenberg, P.A., 1988. Statistical methods for investigating quiescence and other temporal seismicity patterns. Pure Appl. Geophys. 126, 357–372.

Meng, X., Peng, Z., 2014. Seismicity rate changes in the Salton Sea Geothermal Field and the San Jacinto Fault Zone after the 2010 M_w 7.2 El Mayor-Cucapah earthquake. Geophys. J. Int. 197 (3), 1750–1762.

Nicol, A., Beavan, J., 2003. Shortening of an overriding plate and its implications for slip on a subduction thrust, central Hikurangi Margin, New Zealand. Tectonics 22, 1070. https://doi.org/10.1029/2003TC001521.

Parsons, T., 2005. A hypothesis for delayed dynamic earthquake triggering. Geophys. Res. Lett. 32 (4).

Parsons, T., Malagnini, L., Akinci, A., 2017. Nucleation speed limit on remote fluid-induced earthquakes. Sci. Adv. 3 (8), e1700660. https://doi.org/10.1126/sciadv.1700660.

Peng, Z., Zhao, P., 2009. Migration of early aftershocks following the 2004 Parkfield earthquake. Nat. Geosci. 2, 877–881. https://doi.org/10.1038/ngeo697.

Peng, Z., Fry, B., Chao, K., Yao, D., Meng, X., Jolly, A., 2018. Remote triggering of microearthquakes and tremor in New Zealand following the 2016 M7.8 Kaikōura earthquake. Bull. Seismol. Soc. Am. 108 (3B), 1784–1793.

Shelly, D.R., Beroza, G.C., Ide, S., 2007. Non-volcanic tremor and low-frequency earthquake swarms. Nature 446 (7133), 305–307. https://doi.org/10.1038/nature05666.

Shelly, D.R., Peng, Z., Hill, D.P., Aiken, C., 2011. Triggered creep as a possible mechanism for delayed dynamic triggering of tremor and earthquakes. Nat. Geosci. 4, 384–388.

Silver, P., 1998. Why is earthquake prediction so difficult? Seismol. Res. Lett. 69 (2), 111–113.

Todd, E.K., Schwartz, S.Y., Mochizuiki, K., Wallace, L.M., Sheehan, A.F., Webb, S.C., Williams, C.A., Nakai, J., Yarce, J., Fry, B., Henrys, S., Ito, Y., 2018. Earthquakes and tremor linked to seamount subduction during shallow slow slip at the Hikurangi margin, New Zealand. J. Geophys. Res., Solid Earth 123 (8), 6769–6783.

Towns, J., Cockerill, T., Dahan, M., Foster, I., Gaither, K., Grimshaw, A., Hazlewood, V., Lathrop, S., Lifka, D., Peterson, G.D., Roskies, R., Scott, J.R., Wilkins-Diehr, N., 2014. XSEDE: accelerating scientific discovery. Comput. Sci. Eng. 16 (5), 62–74. https://doi.org/10.1109/MCSE.2014.80.

van der Elst, N., Brodsky, E.E., 2010. Connecting near-field and far-field earthquake triggering to dynamic strain. J. Geophys. Res. 115, B07311. https://doi.org/10.1029/2009JB006681.

Wallace, L.M., Beavan, J., McCaffrey, R., Darby, D., 2004. Subduction zone coupling and tectonic block rotations in the North Island, New Zealand. J. Geophys. Res., Solid Earth 109 (B12). https://doi.org/10.1029/2004JB003241.

Wallace, L.M., Beavan, J., 2010. Diverse slow slip behavior at the Hikurangi subduction margin, New Zealand. J. Geophys. Res., Solid Earth 115 (B12), b12402. https://doi.org/10.1029/2010JB007717.

Wallace, L.M., Beavan, J., Bannister, S., Williams, C., 2012. Simultaneous long-term and short-term slow slip events at the Hikurangi subduction margin, New Zealand: implications for processes that control slow slip event occurrence, duration, and migration. J. Geophys. Res., Solid Earth 117, B11402.

Wallace, L.M., Kaneko, Y., Hreinsdottir, S., Hamling, I., Peng, Z., Bartlow, N., D'Anastasio, E., Fry, B., 2017. Large-scale dynamic triggering of shallow slow slip enhanced by overlying sedimentary wedge. Nat. Geosci. 10, 765–770. https://doi.org/10.1038/ngeo3021.

Wallace, L.M., Hreinsdottir, S., Ellis, S., Hamling, I., D'Anastasio, E., Denys, P., 2018. Triggered slow slip and afterslip on the Southern Hikurangi subduction zone following the Kaikōura earthquake. Geophys. Res. Lett. 45 (10), 4710–4718. https://doi.org/10.1002/2018GL077385.

Wang, T., Wei, S., Shi, X., Qiu, Q., Li, L., Peng, D., Weldon, R.J., Barbot, S., 2018. The 2016 Kaikōura earthquake: simultaneous rupture of the subduction interface and overlying faults. Earth Planet. Sci. Lett. 482, 44–51.

Williams, C.A., Eberhart-Phillips, D., Bannister, S., Barker, D.H.N., Henrys, S., Reyners, M., Sutherland, R., 2013. Revised interface geometry for the Hikuangi subduction zone, New Zealand. Seismol. Res. Lett. 84, 6. https://doi.org/10.1785/0220130035.

Wiemer, S., 2001. A software package to analyze seismicity: ZMAP. Seismol. Res. Lett. 72, 373–382.

Xu, W., Feng, G., Meng, L., Zhang, A., Ampuero, J.P., Bürgmann, R., Fang, L., 2018. Transpressional rupture cascade of the 2016 M_w 7.8 Kaikoura earthquake, New Zealand. J. Geophys. Res., Solid Earth 123, 2396–2409.

Yao, D., 2018. Understanding Earthquake Triggering and Fault Slip Behavior Based on Improved Earthquake Catalogs, Doctoral Dissertation, Georgia Institute of Technology, Atlanta, GA.